

Age-Related Change in 5-HT₆ Receptor Availability in Healthy Male Volunteers Measured with ¹¹C-GSK215083 PET

Rajiv Radhakrishnan¹, Nabeel Nabulsi², Edward Gaiser¹, Jean-Dominique Gallezot², Shannan Henry², Beata Planeta², Shu-fei Lin², Jim Ropchan², Wendol Williams¹, Evan Morris^{2,3}, Deepak Cyril D'Souza¹, Yiyun Huang², Richard E. Carson^{2,3}, and David Matuskey^{1,2}

¹Department of Psychiatry, Yale University School of Medicine, New Haven, Connecticut; ²Department of Radiology and Biomedical Imaging, Yale University School of Medicine, New Haven, Connecticut; and ³Department of Biomedical Engineering, Yale University, New Haven, Connecticut

Serotonin receptor 6 (5-hydroxytryptamine-6, or 5-HT₆) is a potential therapeutic target given its distribution in brain regions that are important in depression, anxiety, and cognition. This study sought to investigate the effects of age on 5-HT₆ receptor availability using ¹¹C-GSK215083, a PET ligand with affinity for 5-HT₆ in the striatum and 5-HT_{2A} in the cortex. **Methods:** Twenty-eight healthy male volunteers (age range, 23–52 y) were scanned with ¹¹C-GSK215083 PET. Time-activity curves in regions of interest were fitted using a multilinear analysis method. Nondisplaceable binding potential (BP_{ND}) was calculated using the cerebellum as the reference region and corrected for partial-volume effects. **Results:** In 5-HT₆-rich areas, regional ¹¹C-GSK215083 showed a negative correlation between BP_{ND} and age in the caudate ($r = -0.41$, $P = 0.03$) (14% change per decade) and putamen ($r = -0.30$, $P = 0.04$) (11% change per decade) but not in the ventral striatum or pallidum. A negative correlation with age was also seen in cortical regions ($r = -0.41$, $P = 0.03$) (7% change per decade), consistent with the literature on 5-HT_{2A} availability. **Conclusion:** To our knowledge, this was the first in vivo study on humans to examine the effect of age on 5-HT₆ receptor availability. The study demonstrated a significant age-related decline in 5-HT₆ availability (BP_{ND}) in the caudate and putamen.

Key Words: serotonin 6; age effects; 5-HT₆; PET imaging; ¹¹C-GSK215083

J Nucl Med 2018; 59:1445–1450

DOI: 10.2967/jnumed.117.206516

The 5-hydroxytryptamine-6 (5-HT₆) receptor is a 7-transmembrane serotonin receptor subtype and one of the 14 distinct mammalian serotonin receptors that are expressed almost exclusively in the central nervous system (1,2). In vitro studies demonstrated that 5-HT₆ receptors are localized to the striatum, hippocampus, amygdala, hypothalamus, thalamus, and cerebral cortex (3). The localization to both basal ganglia and limbic structures suggests that this receptor may be involved in the serotonergic control of motor function, mood-dependent behavior, depression, and cognition (3). Subsequently, more attention has recently been given to 5-HT₆

because it presents an attractive therapeutic target for neuropsychiatric disorders.

Functionally, 5-HT₆ exhibits excitatory action, but it can also colocalize with γ -aminobutyric acid-ergic neurons and produce an inhibition of brain activity leading to complicated and discrepant results (2,4). Heterogeneous effects are also seen with other neurotransmitters in specific brain regions, with 5-HT₆ antagonism resulting in increased extracellular glutamate, dopamine, and acetylcholine in the frontal cortex and hippocampus (5,6), whereas 5-HT₆ agonists have been shown to produce increased extracellular γ -aminobutyric acid release in the dorsal hippocampus, striatum, and amygdala (4). Thus, with a multitude of interactions not fully elucidated, preclinical studies on both 5-HT₆ agonists and 5-HT₆ antagonists have shown efficacy against depression, anxiety, and cognitive impairment (1). In addition, 5-HT₆ antagonists have shown promise in the treatment of obesity (7), major depressive disorder (8), age-related cognitive decline (9), and schizophrenia (10). Currently available antidepressants and antipsychotics have also been shown to have a strong affinity for the 5-HT₆ receptor (11,12), adding speculation that these clinical effects might, at least in part, be mediated through this receptor.

Age has been associated with a decline in receptor density across several 5-HT receptor subtypes (13–15). Given that some of the potential indications, such as cognitive impairment in Alzheimer disease and age-related cognitive decline, are related to advancing age, it is important to understand the effects of age on 5-HT₆ receptors and to ascertain whether they remain an important target in older age groups. This importance is further underscored by recent negative results from 2 phase III trials of the 5-HT₆ antagonist idalopirdine for cognitive impairment in Alzheimer disease, despite promising results in preclinical studies (16).

Although age has been shown to be associated with a decline in 5-HT_{1B} (14), 5-HT_{1A}, 5-HT_{2A} (15), and 5-HT₄ receptors (13), the effects of age on 5-HT₆ receptor availability in humans is not known. The availability of a PET ligand for the 5-HT₆ receptor ¹¹C-GSK215083 offers an opportunity to examine the in vivo receptor density in healthy humans and in disease states (17,18). In vitro GSK215083 exhibits high binding affinity for 5-HT₆ ($pK_i = 9.8$) and 5-HT_{2A} ($pK_i = 9.1$) receptors. Although ¹¹C-GSK215083 has high affinity for 5-HT₆ receptors in vivo, it has a nonnegligible affinity (albeit 5-fold lower) for 5-HT_{2A} receptors in cortical regions (17). Therefore, whereas striatal ¹¹C-GSK215083 signal is primarily reflective of 5-HT₆ availability, its binding in the cortex is thought to reflect 5-HT_{2A} availability (17,18).

Received Dec. 4, 2017; revision accepted Mar. 21, 2018.

For correspondence or reprints contact: David Matuskey, Yale University School of Medicine, 801 Howard Ave., New Haven, CT 06520.

E-mail: david.matuskey@yale.edu

Published online Apr. 6, 2018.

COPYRIGHT © 2018 by the Society of Nuclear Medicine and Molecular Imaging.

In this paper, we examine the effects of age on 5-HT₆ receptor availability in healthy male volunteers using the PET ligand ¹¹C-GSK215083.

MATERIALS AND METHODS

Participants

Twenty-eight healthy male volunteers (mean age, 36.0 ± 9.3 y; range, 23–52 y) were included in the study. All underwent a comprehensive screening assessment that included a clinical interview, complete physical examination with medical history, routine blood tests, electrocardiogram, and urine toxicology. Individuals were excluded if they self-reported or evaluation revealed a diagnosis of a current or lifetime psychiatric disorder; current or past serious medical or neurologic illness (including a history of head injury with loss of consciousness); metal in their body, which would result in MRI exclusion; a history of substance abuse or dependence; or illicit drug use in the previous 3 mo.

The study was performed under protocols approved by the Yale Human Investigation Committee, the Yale University Radiation Safety Committee, the Yale–New Haven Hospital Radioactive Drug Research Committee, and the Yale MRI Safety Committee. The study was performed in accordance with good clinical practice guidelines, regulatory requirements, and the code of ethics of the World Medical Association (Declaration of Helsinki). Subjects were recruited from Connecticut and surrounding states by paper and online advertisements, as well as personal referrals. Written informed consent was obtained from all participants at the beginning of screening after the study procedures had been fully explained.

Radiosynthesis of ¹¹C-GSK215083 on the FXC

Automated Module

¹¹C-GSK215083 was radiolabeled with ¹¹C-methyl triflate using an FXC automated module (GE Healthcare) by modifying a previously described procedure (18). ¹¹C-methyl triflate was swept into a solution of desmethyl GSK215083 (0.8–0.9 mg) and 1 μL of 2,2,6,6,-tetramethylpiperidine in 150 μL of anhydrous *N,N*-dimethylformamide and was cooled at –30°C until radioactivity peaked. The resulting solution was then heated at 85°C for 4 min. The reaction mixture was cooled to 50°C, diluted with 1 ml of deionized water, and injected onto the semipreparative high-performance liquid chromatography column (Gemini C18, 5 μm, 10 × 250 mm; Phenomenex Inc.) eluting at a flow rate of 4 mL/min with a mixture of 40% acetonitrile and 60% 0.05 M ammonium formate adjusted to pH 8.1–8.4 using saturated ammonium hydroxide. The radioactivity fraction eluting between 18 and 19 min was collected, diluted with 50 mL of water, and loaded onto a C18 SepPak classic cartridge (Waters). The cartridge was rinsed with 10 mL of 1 mM HCl and dried. The product was then eluted off the SepPak with 1 mL of ethanol (U.S. Pharmacopeia [USP] grade), followed by 3 mL of saline (USP grade), into the product vessel precharged with a mixture of 7 mL of saline (USP grade) and 20 μL of 4.2% sodium bicarbonate (USP grade). The resulting solution was finally passed through a sterile 0.22-μm membrane filter (Millex-MP, 25 mm; Millipore) into a sterile empty dose-vial. Purity and molar activity were determined using an analytic reversed-phase high-performance liquid chromatography column (Luna C18(2), 5 μm, 250 × 4.6 mm; Phenomenex) eluting with a mixture of 40% acetonitrile and 60% 0.1 M ammonium formate at a flow rate of 1.5 mL/min.

Radiosynthesis on the Bioscan AutoLoop

¹¹C-GSK215083 was also radiolabeled with ¹¹C-methyl iodide using a loop method developed at the Yale PET Center. ¹¹C-methyl iodide, produced by the gas-phase method, was swept through the

sample loop preloaded with a solution of 0.5 mg of desmethyl GSK215083 and 1 μL of 2,2,6,6,-tetramethylpiperidine in 80 μL of anhydrous *N,N*-dimethylformamide until radioactivity peaked. The reaction mixture was allowed to stand for 5 min at ambient temperature, loaded onto the semipreparative high-performance liquid chromatography column, and purified as described as above. The product fraction was collected, diluted with 50 mL of water, and loaded onto a C18 Sep-Pak classic cartridge. The cartridge was rinsed with 10 mL of 1 mM HCl and dried. The product was then eluted off the SepPak with 1 mL of ethanol (USP grade), followed by 3 mL of saline (USP grade). The combined solution was finally passed through a sterile 0.22-μm membrane filter into a sterile dose-vial precharged with 7 mL of USP-grade saline and 20 μL of 4.2% sodium bicarbonate (USP grade). Purity and molar activity were determined using a Luna C18(2) column (5 μm, 250 × 4.6 mm) eluting with a mixture of 40% acetonitrile and 60% 0.1 M ammonium formate at a flow rate of 1.5 mL/min.

Image Acquisition

Structural MRI was performed on a 3-T Trio system (Siemens Medical Solutions) with a circularly polarized head coil for purposes of excluding individuals with anatomic abnormalities and anatomically coregistering with PET scans. The dimensions and voxel size of MR images were 256 × 256 × 176 voxels and 0.98 × 0.98 × 1.0 mm, respectively.

Subjects underwent 90-min dynamic PET on an ECAT EXACT HR+ scanner (Siemens Medical Systems) in 3-dimensional mode. Before each PET scan, a transmission scan was acquired for attenuation correction. Up to 740 MBq (20 mCi) of radioactivity were administered by an infusion pump for each scan (mean, 585.39 ± 128.34 MBq). The maximum mass dose from the radioligand was limited to minimize any self-occupancy (≤10 μg) (mean, 3.03 ± 2.32 μg). For each PET scan, ¹¹C-GSK215083 was administered by bolus intravenous infusion over 60 s, immediately followed by acquisition of emission data for up to 90 min.

Arterial input function was measured using an automated blood counter (PBS-101; Veenstra Instruments) for the first 7 min and 15 manual samples between 3 and 90 min after injection. Whole-blood samples were assayed for radioactivity using 0.2 mL, and the rest of the samples were then centrifuged at 2,930g for 5 min to obtain plasma. The radioactivity in all samples was assayed using cross-calibrated γ-counters (1480 Wizard; Perkin-Elmer). Plasma samples collected at 5, 15, 30, 60, and 90 min after injection were mixed with urea to a final concentration of 8 M and were subsequently filtered with 1.0-μm GE Whatman 13-mm CD/X filters. The filtrate was then analyzed with the automatic column-switching high-performance liquid chromatography method (19) to determine the parent fraction and ¹¹C-GSK215083 metabolites.

Metabolite Analysis

Injected samples were first eluted through a capture column hand-packed with C18 sorbent (Strata-X; Phenomenex) using a mobile phase of 1:99 MeCN:H₂O (v/v) at 2 mL/min for 4 min. The capture column was then backflushed onto the analytical column (Phenomenex Luna C18(2), 4.6 × 250 mm, 5 μm) with a mobile phase of 40:60 MeCN:0.1 M ammonium formate at a flow rate of 1.4 mL/min, giving a retention time of 8.5 min for parent ¹¹C-GSK215083. Eluent was collected in separate vials every 2 min with a fraction collector (CF-1; Spectrum Chromatography) and counted with γ-counters. The time course of the unchanged (i.e., parent) fraction in the filtrate was fit with an integrated γ-function. This fraction curve was corrected for the time-varying extraction efficiency of radioactivity. The final plasma input function was calculated as the product of the total plasma time–activity curve and the parent

fraction curve. Plasma free fraction was assessed by ultrafiltration (Centrifree; MilliporeSigma). The plasma free fraction was determined as the ratio of the radioactivity concentration in the filtrate to the total activity in plasma. Measurements of free fraction were performed in triplicate for each scan.

Image Processing

Dynamic scan data were reconstructed with corrections for attenuation, normalization, scatter, random events, and dead time using ordered-subsets expectation maximization (4 iterations, 16 subsets). PET images were reconstructed into 27 frames containing 63 axial slices of 128×128 voxels each ($2.1 \times 2.1 \times 2.4$ mm). Motion correction was applied to the dynamic images using a mutual-information algorithm (FSL-FLIRT, version 3.2; FMRIB Analysis Group) by frame-by-frame registration to a summed image (0–10 min after injection). A summed image was created from the motion-corrected data and registered to the subject's 3-T MR anatomic image (6-parameter affine registration), which was then registered to an MRI template using a nonlinear transform with BioImage Suite. Regions of interest (ROIs) were based on anatomic automatic labeling for SPM2 (20) with the exception of a ventral striatum ROI that was drawn manually on each individual MR image (21,22). Time–activity curves were then generated in all ROIs.

Time–activity curves were fitted with the MA1 (multilinear analysis 1) method of Ichise et al. (23) ($t^* = 40$) using the metabolite-corrected arterial input function over 90 min after injection. Volumes of distribution were estimated for the amygdala, cerebellum, caudate, hippocampus, putamen, pallidum, and ventral striatum and for a global cortical region consisting of the frontal, parietal, temporal, and occipital cortices. Regional nondisplaceable binding potential (BP_{ND}) was calculated from distribution volumes using cerebellum as the reference region because it is virtually devoid of 5-HT_{2A} (24) and 5-HT₆ receptors (25).

Partial-volume correction based on the Mueller-Gartner algorithm (26) was applied after segmentation of MR images using SPM12. The uncorrected and corrected data were analyzed separately.

Because striatal ¹¹C-GSK215083 BP_{ND} primarily reflects 5-HT₆ availability, a linear mixed model (SPSS Statistics for Macintosh, version 22.0; IBM) was used to model the independent and joint effects of age (continuous) and striatal ROIs (i.e., caudate, putamen, and ventral striatum) (within-subject factor) on BP_{ND} , with intercept as a random effect, a scaled identity covariance structure, and relevant covariates of body mass index (BMI) and mass dose (μ g). The interaction between region and age was modeled, and slopes for regions were estimated post hoc. Correlations between age and BP_{ND} were calculated separately for each region, and P values unadjusted for multiple comparisons are reported.

RESULTS

Table 1 shows the demographics of the study sample.

The results of the primary mixed-model analysis on striatal ROIs (uncorrected BP_{ND}), with BMI and mass dose as covariates, showed an overall significant effect of age ($F_{(1,24)} = 7.39$, $P = 0.012$), ROIs ($F_{(2,52)} = 5.35$, $P = 0.008$) and an age \times ROI interaction ($F_{(2,52)} = 5.07$, $P = 0.010$). There was no main effect of BMI or mass dose. Similarly, after partial-volume correction, analysis with BMI and mass dose as covariates showed a significant effect of age ($F_{(1,24)} = 5.93$, $P = 0.02$) and ROI ($F_{(2,52)} = 10.67$, $P < 0.001$) but no age \times ROI interaction ($F_{(2,52)} = 2.83$, $P = 0.07$). There was also no main effect of either BMI or mass dose with partial-volume correction.

TABLE 1
Demographics of Sample

Demographic	Data
Age (y)	36.00 \pm 9.26
Height (m)	1.78 \pm 0.05
Weight (kg)	83.47 \pm 9.48
BMI	26.33 \pm 2.61
Male	100%
Ethnicity	
White	28.6%
African-American	57.1%
Hispanic	10.7%
Other	3.6%

Data are mean \pm SD or percentage.

To verify that age effect on BP_{ND} was not confounded by age-related changes in the reference region, we examined the correlation between age and cerebellar distribution volume and found no significant correlation ($r = 0.04$, $P = 0.85$).

Table 2 presents average ¹¹C-GSK215083 BP_{ND} (with SD) for ROIs, along with the correlation with age, the percentage change per decade, slope (change in BP_{ND} per year), and the unadjusted P value. BP_{ND} was comparable to that estimated using MA2 by Parker et al. (18). ¹¹C-GSK215083 BP_{ND} correlated negatively with age in the caudate (corrected: $r = -0.44$, $P = 0.02$; uncorrected: $r = -0.62$, $P = 0.001$), putamen (corrected: $r = -0.42$, $P = 0.03$; uncorrected: $r = -0.44$, $P = 0.02$), and cortical regions (corrected: $r = -0.47$, $P = 0.01$; uncorrected: $r = -0.62$, $P = <0.001$) but not in the amygdala, hippocampus, ventral striatum, or pallidum (Table 2; Fig 1). The reduction per decade was 18% in the caudate, 10% in the putamen, and 12% in cortical regions with the uncorrected BP_{ND} data. Likewise, with the corrected BP_{ND} data, similar reductions were found: 14% in the caudate, 11% in the putamen, and 7% in cortical regions.

DISCUSSION

To our knowledge, this was the first in vivo study on humans to examine the effects of age on 5-HT₆ receptor availability (BP_{ND}) using ¹¹C-GSK215083 PET imaging. The study demonstrated the presence of a significant age-related decline in 5-HT₆ availability in the caudate and putamen but not in the amygdala, hippocampus, ventral striatum, or pallidum. The reduction per decade was greatest in the caudate (14%) followed by the putamen (11%) in corrected data. ¹¹C-GSK215083 binding in cortical regions, reflective of 5-HT_{2A} availability, also showed an age-related decline (7% per decade).

Consistent with a prior autoradiography study on humans (11) and a PET imaging study using ¹¹C-GSK215083 (18), 5-HT₆ availability was found to be higher in striatal than nonstriatal regions. ¹¹C-GSK215083 has significant affinity for 5-HT_{2A} receptors in cortical regions (17). In a series of displacement studies using a 5-HT_{2A}-selective antagonist (ketanserin) and a dual 5-HT₆/5-HT_{2A} antagonist (SB742457), Parker et al. (18) demonstrated that

TABLE 2
Regional ^{11}C -GSK215083 BP_{ND} and Correlation with Age

ROI	Mean $BP_{\text{ND}} \pm \text{SD}$	Correlation with age	Change per decade	Slope	P (unadjusted)
Uncorrected data					
Amygdala	0.37 \pm 0.11	-0.05	-1.7%	-0.0006	0.79
Caudate	1.08 \pm 0.40	-0.62	-17.5%	-0.0262	0.001*
Hippocampus	0.28 \pm 0.12	-0.24	-9.4%	-0.0031	0.22
Putamen	1.51 \pm 0.37	-0.44	-9.8%	-0.0176	0.02*
Pallidum	0.84 \pm 0.24	-0.09	-2.7%	-0.0024	0.64
Ventral striatum	1.20 \pm 0.44	-0.17	-6.1%	-0.0082	0.38
Global cortical ROI	0.48 \pm 0.11	-0.62	-12.0%	-0.0071	<0.001*
Partial-volume corrected data					
ROI					
Amygdala	0.26 \pm 0.10	-0.09	-3.5%	-0.0010	0.66
Caudate	1.58 \pm 0.60	-0.44	-14.1%	-0.0286	0.02*
Hippocampus	0.24 \pm 0.15	-0.26	-13.1%	-0.0041	0.19
Putamen	1.63 \pm 0.50	-0.42	-11.3%	-0.0225	0.03*
Pallidum	1.59 \pm 0.60	0.07	2.8%	0.0042	0.74
Ventral striatum	1.02 \pm 0.45	-0.23	-9.2%	-0.0110	0.25
Global cortical ROI	1.05 \pm 0.16	-0.47	-7.1%	-0.0084	0.01*

*Statistically significant.

cortical ^{11}C -GSK215083 BP_{ND} was primarily reflective of 5-HT_{2A} availability.

The finding of an age-related decline in 5-HT₆ receptor availability is largely consistent with other 5-HT receptors, namely 5-HT_{1A}, 5-HT_{1B}, 5-HT_{2A}, and 5-HT₄ (13,14,27,28), although there are regional differences. The age-related decline in cortical ^{11}C -GSK215083 BP_{ND} (reflective of 5-HT_{2A} receptor availability) is consistent with previous PET imaging studies using other selective or nonselective radiotracers (15,28). Moses-Kolko et al. (15) found an 8% decline per decade in 5-HT_{2A} availability using ^{18}F -altanserin, a finding that is strikingly similar to our finding of a 7% decline per decade in corrected data. A similar pattern of age-related decline in cortical areas has also been seen with 5-HT_{1A} (15) and 5-HT_{1B} receptors (14).

The region-specific age-related decline in the caudate and putamen, but not in the amygdala, hippocampus, ventral striatum, or pallidum, is a unique finding. This result persisted despite controlling for potential confounders such as BMI and mass dose and correcting for partial-volume effects. We also performed a secondary analysis excluding outliers (defined as $BP_{\text{ND}} > 3$ SDs from mean). The BP_{ND} of 3.9 in the caudate was more than 3 SDs from the mean, and when this value was excluded, the overall results in the caudate were similar, demonstrating a significant age-related decline ($y = -0.0170 + 2.1106$; $r = -0.39$, $P = 0.041$).

Among the 5-HT receptor subtypes, age-related decline in the caudate and putamen has been observed with 5-HT_{2A} (28) and 5-HT₄ (exclusively in the striatum; not in cortical areas) (13), whereas 5-HT_{1B} showed an increase in availability with age in the pallidum and putamen (14).

An age-related decline in 5-HT_{2A} receptor availability has been shown in the hippocampus and amygdala (15). Because both

5-HT_{2A} and 5-HT₆ receptors are expressed in the amygdala (29,30) and hippocampus (31,32), the absence of an age effect in these ROIs in our study could be confounded by the relative proportion of 5-HT₆ and 5-HT_{2A} receptors, low BP_{ND} , or high variability in these small ROIs. Therefore, specific conclusions on changes in 5-HT₆ receptor availability with age in these regions cannot be drawn from our present results.

The findings of the study must be viewed within the context of its limitations. Our sample comprised male subjects who were younger than 60 y, with a mean of 36.0 ± 9.3 y. The sample thus does not capture age effects in subjects older than 60 y, and it would be important to include older subjects in future studies.

Another limitation is that the ligand, GSK215083, has high affinity for both 5-HT_{2A} and 5-HT₆ receptors. It is therefore difficult to ascribe a change in tracer binding to one specific receptor type. To more accurately estimate the effect of age on 5-HT₆ receptor density with ^{11}C -GSK215083, a blocking study could be done with a selective 5-HT_{2A} antagonist. A previous study showed that ketanserin, a 5-HT_{2A} antagonist, reduced only 3% of ^{11}C -GSK215083 signal in the putamen and 16% in the caudate (18). On the basis of this finding, the signal in the putamen and caudate in the current work is thought to reflect relatively specific binding for the 5-HT₆ receptor.

Additionally, whereas the MA2 reference model is a validated method for the ligand (18), the MA1 reference model was found to be a good fit for time-activity curves in our sample, in part, by only fitting data for times longer than 40 min. There were no significant age effects on cerebellar distribution volume, and therefore the use of cerebellum as a reference region does not confound the results. The age-related decline in 5-HT₆ receptor availability in caudate and putamen is an important consideration for drug

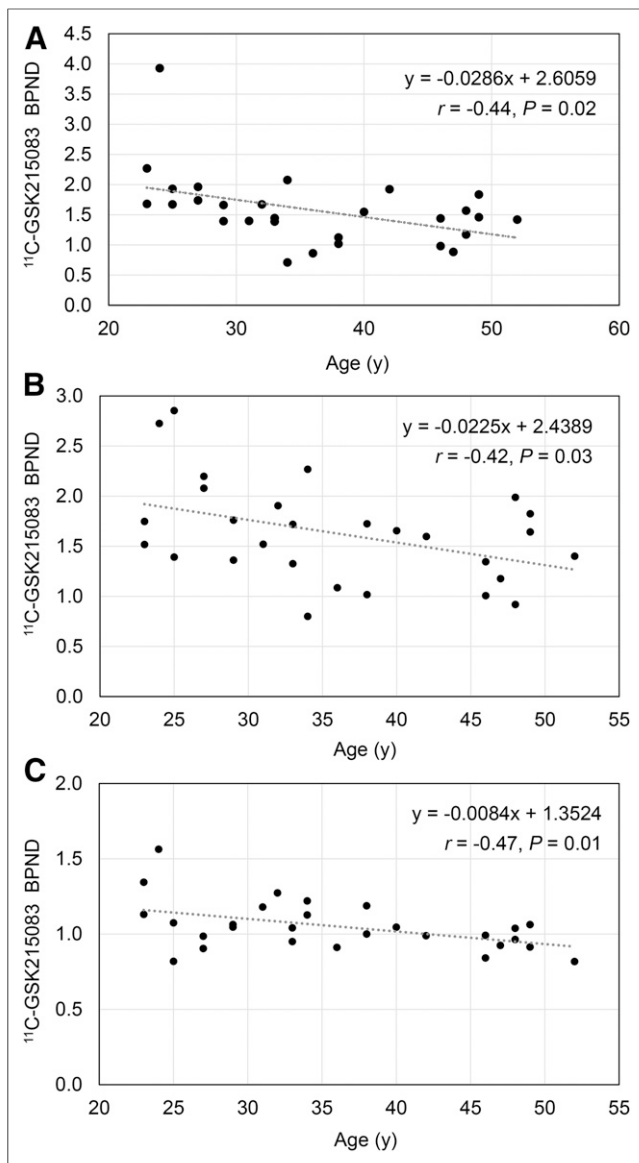


FIGURE 1. Correlation between age and ^{11}C -GSK215083 BP_{ND} in caudate (A), putamen (B), and cortical (C) regions.

development aimed at targeting this receptor in the treatment of geriatric depression, age-related cognitive decline, and movement disorders.

CONCLUSION

This in vivo study on humans examined the effect of age on 5-HT₆ receptor availability and found a significant age-related decline in 5-HT₆ availability (BP_{ND}) in the caudate and putamen.

DISCLOSURE

This work was supported by Abbvie and Pfizer. Rajiv Radhakrishnan is supported by the David Mahoney grant program of the Dana Foundation and by CTSA grant UL1 TR001863 from the National Center for Advancing Translational Science (NCATS), components of the National Institutes of Health (NIH), and the NIH Roadmap for Medical Research. No other potential conflict of interest relevant to

this article was reported. The contents of this publication are solely the responsibility of the authors and do not necessarily represent the official view of NIH.

ACKNOWLEDGMENTS

We thank the staff of the Yale PET Center, the Clinical Neuroscience Research Unit (CNRU) at the Connecticut Mental Health Center (CMHC) of the Connecticut Department of Mental Health and Addiction Services (DMHAS), the Hospital Research Unit (HRU) at Yale–New Haven Hospital (YNHH), and the Yale Magnetic Resonance Research Center (MRRC).

REFERENCES

1. Yun HM, Rhim H. The serotonin-6 receptor as a novel therapeutic target. *Exp Neurol.* 2011;20:159–168.
2. Borsini F, Bordi F, Riccioni T. 5-HT₆ pharmacology inconsistencies. *Pharmacol Biochem Behav.* 2011;98:169–172.
3. Hirst WD, Abrahamsen B, Blaney FE, et al. Differences in the central nervous system distribution and pharmacology of the mouse 5-hydroxytryptamine-6 receptor compared with rat and human receptors investigated by radioligand binding, site-directed mutagenesis, and molecular modeling. *Mol Pharmacol.* 2003; 64:1295–1308.
4. Schechter LE, Lin Q, Smith DL, et al. Neuropharmacological profile of novel and selective 5-HT₆ receptor agonists: WAY-181187 and WAY-208466. *Neuropsychopharmacology.* 2008;33:1323–1335.
5. Hirst WD, Stean TO, Rogers DC, et al. SB-399885 is a potent, selective 5-HT₆ receptor antagonist with cognitive enhancing properties in aged rat water maze and novel object recognition models. *Eur J Pharmacol.* 2006;553: 109–119.
6. Shirazi-Southall S, Rodriguez DE, Nomikos GG. Effects of typical and atypical antipsychotics and receptor selective compounds on acetylcholine efflux in the hippocampus of the rat. *Neuropsychopharmacology.* 2002; 26:583–594.
7. Dudek M, Marcinkowska M, Bucki A, Olczyk A, Kolaczowski M. Idalopirdine: a small molecule antagonist of 5-HT₆ with therapeutic potential against obesity. *Metab Brain Dis.* 2015;30:1487–1494.
8. Abraham R, Nirogi R, Shinde A. Role of glutamate and advantages of combining memantine with a 5HT₆ ligand in a model of depression. *Pharmacol Rep.* 2014; 66:394–398.
9. Callaghan CK, Hok V, Della-Chiesa A, Virley DJ, Upton N, O'Mara SM. Age-related declines in delayed non-match-to-sample performance (DNMS) are reversed by the novel 5HT₆ receptor antagonist SB742457. *Neuropharmacology.* 2012;63:890–897.
10. Morozova MA, Lepilkina TA, Rupchev GE, et al. Add-on clinical effects of selective antagonist of 5HT₆ receptors AVN-211 (CD-008-0173) in patients with schizophrenia stabilized on antipsychotic treatment: pilot study. *CNS Spectr.* 2014;19:316–323.
11. East SZ, Burnet PW, Leslie RA, Roberts JC, Harrison PJ. 5-HT₆ receptor binding sites in schizophrenia and following antipsychotic drug administration: autoradiographic studies with [¹²⁵I]SB-258585. *Synapse.* 2002;45:191–199.
12. Monsma FJ Jr, Shen Y, Ward RP, Hamblin MW, Sibley DR. Cloning and expression of a novel serotonin receptor with high affinity for tricyclic psychotropic drugs. *Mol Pharmacol.* 1993;43:320–327.
13. Madsen K, Haahr MT, Marnier L, et al. Age and sex effects on 5-HT₄ receptors in the human brain: a [¹¹C]SB207145 PET study. *J Cereb Blood Flow Metab.* 2011;31:1475–1481.
14. Matuskey D, Pittman B, Planeta-Wilson B, et al. Age effects on serotonin receptor 1B as assessed by PET. *J Nucl Med.* 2012;53:1411–1414.
15. Moses-Kolko EL, Price JC, Shah N, et al. Age, sex, and reproductive hormone effects on brain serotonin-1A and serotonin-2A receptor binding in a healthy population. *Neuropsychopharmacology.* 2011;36:2729–2740.
16. Ferrero H, Solas M, Francis PT, Ramirez MJ. Serotonin 5-HT₆ receptor antagonists in Alzheimer's disease: therapeutic rationale and current development status. *CNS Drugs.* 2017;31:19–32.
17. Parker CA, Gunn RN, Rabiner EA, et al. Radiosynthesis and characterization of ¹¹C-GSK215083 as a PET radioligand for the 5-HT₆ receptor. *J Nucl Med.* 2012;53:295–303.

18. Parker CA, Rabiner EA, Gunn RN, et al. Human kinetic modeling of the 5HT₆ PET radioligand ¹¹C-GSK215083 and its utility for determining occupancy at both 5HT₆ and 5HT_{2A} receptors by SB742457 as a potential therapeutic mechanism of action in Alzheimer disease. *J Nucl Med.* 2015;56:1901–1909.
19. Hilton J, Yokoi F, Dannals RF, Ravert HT, Szabo Z, Wong DF. Column-switching HPLC for the analysis of plasma in PET imaging studies. *Nucl Med Biol.* 2000;27:627–630.
20. Tzourio-Mazoyer N, Landeau B, Papathanassiou D, et al. Automated anatomical labeling of activations in SPM using a macroscopic anatomical parcellation of the MNI MRI single-subject brain. *Neuroimage.* 2002;15:273–289.
21. Gaiser EC, Gallezot JD, Worhunsky PD, et al. Elevated dopamine D_{2/3} receptor availability in obese individuals: a PET imaging study with [¹¹C](+)PHNO. *Neuropsychopharmacology.* 2016;41:3042–3050.
22. Mawlawi O, Martinez D, Slifstein M, et al. Imaging human mesolimbic dopamine transmission with positron emission tomography: I. Accuracy and precision of D₂ receptor parameter measurements in ventral striatum. *J Cereb Blood Flow Metab.* 2001;21:1034–1057.
23. Ichise M, Toyama H, Innis RB, Carson RE. Strategies to improve neuroreceptor parameter estimation by linear regression analysis. *J Cereb Blood Flow Metab.* 2002;22:1271–1281.
24. Hall H, Farde L, Halldin C, Lundkvist C, Sedvall G. Autoradiographic localization of 5-HT(2A) receptors in the human brain using [³H]M100907 and [¹¹C]M100907. *Synapse.* 2000;38:421–431.
25. Roberts JC, Reavill C, East SZ, et al. The distribution of 5-HT₆ receptors in rat brain: an autoradiographic binding study using the radiolabelled 5-HT₆ receptor antagonist [¹²⁵I]SB-258585. *Brain Res.* 2002;934:49–57.
26. Giovacchini G, Lerner A, Toczek MT, et al. Brain incorporation of ¹¹C-arachidonic acid, blood volume, and blood flow in healthy aging: a study with partial-volume correction. *J Nucl Med.* 2004;45:1471–1479.
27. Costes N, Merlet I, Ostrowsky K, et al. A ¹⁸F-MPPF PET normative database of 5-HT_{1A} receptor binding in men and women over aging. *J Nucl Med.* 2005;46:1980–1989.
28. Uchida H, Chow TW, Mamo DC, et al. Effects of aging on 5-HT_{2A} R binding: a HRRT PET study with and without partial volume corrections. *Int J Geriatr Psychiatry.* 2011;26:1300–1308.
29. Dwivedi Y, Pandey GN. Quantitation of 5HT_{2A} receptor mRNA in human post-mortem brain using competitive RT-PCR. *Neuroreport.* 1998;9:3761–3765.
30. Kindlundh-Högberg AM, Svenningsson P, Schiöth HB. Quantitative mapping shows that serotonin rather than dopamine receptor mRNA expressions are affected after repeated intermittent administration of MDMA in rat brain. *Neuropharmacology.* 2006;51:838–847.
31. Liu KC, Li JY, Tan HH, et al. Serotonin₆ receptors in the dorsal hippocampus regulate depressive-like behaviors in unilateral 6-hydroxydopamine-lesioned Parkinson's rats. *Neuropharmacology.* 2015;95:290–298.
32. Collins SA, Huff C, Chiaia N, Gudelsky GA, Yamamoto BK. 3,4-methylenedioxymethamphetamine increases excitability in the dentate gyrus: role of 5HT_{2A} receptor-induced PGE₂ signaling. *J Neurochem.* 2016;136:1074–1084.